molecular pharmaceutics

articles

Tracking the Relative In Vivo Pharmacokinetics of Nanoparticles with PARACEST MRI

M. Meser Ali,[†] Byunghee Yoo,[‡] and Mark D. Pagel*[,‡,§]

Department of Radiology, Henry Ford Health System, Detroit, Michigan, and Biomedical Engineering Interdisciplinary Program, and Department of Chemistry, University of Arizona, Tucson, Arizona

Received February 2, 2009; Revised Manuscript Received March 18, 2009; Accepted March 19, 2009

Abstract: A noninvasive assay that tracks the relative in vivo pharmacokinetics of two nanoparticles may accelerate the development of nanoparticles for biomedical applications, and may provide a method to select personalized nanomedicines for individual patients. To develop an in vivo competitive assay, two MRI contrast agents that could be selectively detected through paramagnetic chemical exchange saturation transfer (PARACEST) were conjugated to a second generation and fifth generation polyamidoamine (PAMAM) dendrimer. The CEST effects of each agent was calibrated relative to concentration. The effects of T_1 relaxivities of these dendritic PARACEST magnetic resonance imaging (MRI) contrast agents were found to be negligible relative to their CEST effects with respect to changes in image contrast, which facilitated the measurement of the ratios of their chemical exchange lifetimes. Injection of both contrast agents into a mouse model of mammary carcinoma resulted in a temporal increase in the CEST effect from each agent in the flank tumor. Although the in vivo CEST effects could not be used to determine the absolute concentrations of each agent within the tumor, the ratio of the in vivo CEST effects was used to measure the ratio of the concentrations of the agents. This result demonstrated that the relative in vivo pharmacokinetics of two nanoparticles may be evaluated using PARACEST MRI.

Keywords: MRI; dendrimers; contrast agents; pharmacokinetics; breast cancer

Introduction

The emerging field of nanomedicine has rapidly developed a variety of nanopaticles for medical applications, including dendrimers, liposomes, nanoshells, nanotubes, emulsions, and quantum dots.[1] The physical and chemical properties of these nanoparticles can be modified to customize the pharmacokinetic delivery of the nanoparticle to pathological tissue targets.[2] As a longer-term goal, the properties of nanoparticles should be tuned to the pharmcokinetic properties of individual patients as part of the paradigm of personalized medicine.[3] To achieve these goals, noninvasive methods are required to assess the pharmacokinetics of nanoparticles in order to further optimize their tissue-targeting properties, and to tune their properties for individual patients. Ideally, these noninvasive methods should selectively detect two or more nanoparticles during the same pharmacokinetic study in order to perform an in vivo competitive assay that can identify the best nanoparticles for each biomedical application.

* Corresponding author. Mailing address: Arizona Cancer Center, room 4949B, 1515 N. Campbell Ave., Tucson, AZ 85724-5024. Telephone: 520-404-7049. Fax: 520-626-0395. E-mail: mpagel@u.arizona.edu.

[†] Henry Ford Health System.

[‡] Biomedical Engineering Interdisciplinary Program, University of Arizona.

[§] Department of Chemistry, University of Arizona.

(1) Caruthers, S. D.; Wickline, S. A.; Lanza, G. M. Nanotechnological applications in medicine. *Curr. Opin. Biotechnol.* **2007**, *18* (1), 26–30.

(2) Brannon-Peppas, L.; Blanchette, J. O. Nanoparticle and targeted systems for cancer therapy. *Adv. Drug Delivery Rev.* **2004**, *56* (11), 1649–1659.

(3) Jain, K. K. Role of nanobiotechnology in developing personalized medicine for cancer. *Technol. Cancer Res. Treat.* **2005**, *4*, 645–650.

10.1021/mp900040u CCC: $40.75 © 2009 American Chemical Society
Published on Web 03/19/2009

Magnetic resonance imaging (MRI) can track the pharmacokinetics of metal-carrying nanoparticles in preclinical and clinical studies. Metals such as gadolinium can change the T_1 and T_2 relaxation rates of tissue water, and other metals such as iron can change T_2* relaxation rates, which lead to a change in T_1-weighted or T_2*-weighted image contrast.[4] This change in image contrast can be used to determine the concentration of the agent, which can be used to measure the in vivo pharmacokinetics of the agent.[5] Unfortunately, two or more T_1-, T_2-, or T_2*-relaxation MRI contrast agents cannot be selectively detected during a single pharmacokinetic study. Although the selective detection of one T_1 MRI contrast agent and one T_2* MRI contrast agent is feasible, the strong correlations between T_1- and T_2*-relaxation require careful calibrations to differentiate and quantify both relaxation effects.[6]

During the past decade, MRI contrast agents have been developed that can be selectively detected through chemical exchange saturation transfer (CEST).[7] These contrast agents contain protons that undergo chemical exchange with protons of surrounding water molecules, such as protons in amine or amide groups in the covalent structure of the agent, or protons in water molecules that are noncovalently bound to the contrast agent.[8,9] A narrow band of radio frequencies that are applied at the chemical shift of the exchangeable proton of the CEST agent can selectively saturate the MR signal of the proton, so that the MR signal is eliminated. Subsequent chemical exchange of the saturated proton on the CEST agent with a proton on a water molecule transfers the saturation to the water, which reduces the total detectable MR signal of water. Paramagnetic CEST (PARACEST) agents contain lanthanide ions that increase the chemical shifts of their exchangeable protons, which greatly facilitates the selective detection of each agent in the presence of other agents.[8−10]

This report investigates the utility of using PARACEST MRI contrast agents to detect the pharmacokinetics of two nanopaticles during a single MRI study. Polyamidoamine (PAMAM) dendrimers were selected as a model nanoparticle for this study, because these dendrimers have well-controlled sizes and well-characterized purities.[11] These dendrimers have excellent chemical functionality for conjugation to MRI contrast agents, and are biocompatible when the cationic surface is neutralized by conjugation to anionic MRI contrast agents.[12] These dendrimers can carry a high density of MRI contrast agent, and can expose each agent to surrounding water to generate a strong MRI signal, which is essential for the study of PARACEST agents that typically show marginal sensitivities for in vivo applications. A mouse model of mammary carcinoma was selected for the in vivo study, based on the known difference in pharmacokinetics of dendritic MRI contrast agents with different hydrodynamic diameters in this type of tissue.[13]

Experimental Section

Synthesis and Characterization. DOTA-Gly, the tetraglycineamide derivative of 1,4,7,10-tetraazacyclododecane-1,4,7,10-tetraacetic acid (DOTA), was synthesized using a previously reported method.[10] To chelate Eu(III) or Yb(III), DOTA-Gly (633 mg, 1 mmol) was dissolved in water (5 mL) at pH 6.5 and 40 °C, and 3 mL of $EuCl_3$ (258 mg, 1 mmol) or $YbCl_3$ (273 mg, 1 mmol) in water was added dropwise for 1 h while controlling pH at 7.5 with 0.1 N NaOH. The solution was stirred for 12 h at 60 °C, the pH was adjusted to 9 at room temperature, and residual lanthanide-hydroxide white precipitate was removed by filtration. The complete complexation was evaluated with an Arsenazo III color test, which showed negative results for free lanthanide ions. The solution was freeze-dried, yielding Eu-DOTA-Gly (697 mg, yield: 88.8%) or Yb-DOTA-Gly (755 mg, yield: 94.5%).

To synthesize a large dendritic PARACEST agent, EDC (0.34 g, 1.77 mmol), NHS (0.82 g, 0.70 mmol), and DOTA-Gly (0.26 g, 0.40 mmol) were dissolved in MES buffer (25 mL of 0.1 M MES at pH 6.5) and stirred at 0 °C for 1 h. A fifth generation PAMAM dendrimer (G5PAMAM; 40 mg, 1.4 μmol) was dissolved in DMSO/H_2O (1:1) and was slowly

(4) Merbach, A. F.; Toth, E. *The chemistry of contrast agents in medical magnetic resonance imaging*; John Wiley & Sons Inc.: New York, 2001.

(5) Tweedle, M. F.; Eaton, S. M.; Eckelman, W. C.; Gaughan, G. T.; Hagan, J. J.; Wedeking, P. W.; Yost, F. J. Comparative chemical structure and pharmacokinetics of MRI contrast agents. *Invest. Radiol.* **1988**, *23* (Suppl. 1), S236–S239.

(6) Zhang, X.; Martinez, G. V.; Garcia-Martin, M. L.; Woods, M.; Sherry, A. D.; Gillies, R. J. In Vivo pHe Measurement with a Relaxometric pH Sensitive Contrast Agent. *Proc. World Mol. Imaging Congr.* **2008**; 0481.

(7) Ward, K. M.; Aletras, A. H.; Balaban, R. S. A new class of contrast agents for MRI based on proton chemical exchange dependent saturation transfer (CEST). *J. Magn. Reson.* **2000**, *143*, 79–87.

(8) Zhang, S.; Michaudet, L.; Burgess, S.; Sherry, A. D. The amide protons of an Ytterbium(III) dota tetraamide complex act as efficient antennae for transfer of magnetization to bulk water. *Angew. Chem., Int. Ed.* **2002**, *114* (11), 1999–2001.

(9) Zhang, S.; Winter, P.; Wu, K.; Sherry, A. D. A novel europium(III)-based MRI contrast agent. *J. Am. Chem. Soc.* **2001**, *123*, 1517–1518.

(10) Aime, S.; Barge, A.; Delli Castelli, D.; Fedeli, F.; Mortillaro, A.; Nielsen, F. U.; Terreno, E. Paramagnetic lanthanide(III) complexes as pH-sensitive chemical exchange saturation transfer (CEST) contrast agents for MRI applications. *Magn. Reson. Med.* **2002**, *47*, 639–648.

(11) Ali, M. M.; Woods, M.; Caravan, P. C.; Opina, A.; Spiller, A.; James, C.; Sherry, A. D. Synthesis and relaxometric studies of a dendrimer-based pH responsive MRI contrast agent. *Chem.—Eur. J.* **2008**, *14*, 7250–7258.

(12) Pikkemaat, J. A.; Wegh, R. T.; Lamerichs, R.; van de Molengraaf, R. A.; Sangereis, S.; Burdinski, D.; Raymond, A. Y. F.; Janssen, H. M.; de Waal, B. F. M.; Willard, N. P.; Meijer, E. W.; Grull, H. Dendritic PARACEST contrast agents for magnetic resonance imaging. *Contrast Media Mol. Imaging* **2007**, *2*, 229–239.

(13) Kobayashi, H.; Brechbiel, M. W. Dendrimer-based macromolecular MRI contrast agents: characteristics and application. *Mol. Imaging* **2003**, *2* (1), 1–10.

added to the reaction mixture and further stirred for 24 h at room temperature. The product was repeatedly filtered through a Centricon C-30 diafiltration cell with a 30 kD MWCO until SEC-HPLC revealed that no further low molecular weight material was present. The retentate was lyophilized to obtain 0.07 g of a colorless solid. This procedure was repeated to couple additional DOTA-Gly to the same G5-PAMAM dendrimer, which resulted in 0.13 g of a colorless solid that was characterized with a MALDI mass spectrometer. A total of 1.2 equiv of $EuCl_3$ in H_2O was added to a solution of $(DOTA\text{-}Gly)_{41}$-G5PAMAM in H_2O (pH 6−7). After stirring at 40 °C for 48 h, EDTA was added to remove free metal ions, and the product was repeatedly filtered through a 250 mL diafiltration cell with a 10 kDa MWCO until SEC-HPLC revealed that no further low molecular weight material was present. The retentate was lyophilized to obtain the final large dendritic PARACEST agent, $(Eu\text{-}DOTA\text{-}Gly)_{41}$-G5PAMAM (Eu-G5), with 70% yield, which was characterized for lanthanide ion content with ICP-mass spectrometry.

To synthesize a small dendritic PARACEST agent, the same synthesis procedure was used to couple DOTA-Gly to a second generation PAMAM dendrimer (G2PAMAM; 40 mg, 12.18 μmol; Dendritech Inc., Midland, MI), using a Centricon C-3 diafilration cell with a 3 kD MWCO. The retentate was lyophilized to obtain 0.15 g of a colorless solid that was characterized with a MALDI mass spectrometer. The same chelation procedure was used to obtain the final small dendritic PARACEST agent, $(Yb\text{-}DOTA\text{-}Gly)_6$-G2PAMAM (Yb-G2), with 75% yield by using $YbCl_3$ and a diafiltration cell with a 3 kDa MWCO, which was characterized for lanthanide ion content with ICP-mass spectrometry.

The Calibration of CEST with Concentration. Solutions were prepared with 5−40 mM Eu-DOTA-Gly, 1.57−25 mM Yb-DOTA-Gly, 0.0195−0.3125 mM Eu-G5, and 0.234−1.875 mM Yb-G2. MRI scans of the solutions were performed with a 9.4T Bruker Biospec small animal MRI scanner equipped with a 35 mm birdcage RF coil. A RARE MRI pulse sequence with a RARE factor of 16 (TR/TE= 4.0 s/8.01 ms) was prepended with a saturation period that consisted of a train of Gaussian pulses applied with a 20 μT saturation power for 2.27 s. A total of 38 s was required to acquire a single MR image with 128 × 128 pixels that covered a 35 × 35 mm field of view, a single slice with a thickness of 1 mm, and a single average. The water signal was measured for each phantom when saturation was applied at 55 ppm (M_s) and −55 ppm (M_0) to measure the CEST effect of Eu-G5, and at −16 ppm (M_s) and +16 ppm (M_0) to measure the CEST effect of Yb-G2 (see eq 1 for a description of M_s and M_0). The temperature was maintained at 37 °C during all CEST NMR studies using warmed air and a computer-controlled temperature feedback system (SA Instruments, Inc.).

Steady-state chemical exchange between water and an exchangeable proton on a CEST agent can be described by a simple two-pool model. The Bloch equations that describe MRI signals can be modified to include this chemical exchange (eq 1).[14] These properties include the T_1 relaxation time of the water in the presence of the agent, which is linearly dependent on the concentration of the agent (eq 2).[4] The two-pool MR CEST equation was rearranged to form a linear equation, which was analogous to the rearrangement of the Michaelis Menten enzyme kinetics equation to form a linear Hanes equation (eq 3).[15] This linear relationship was evaluated using the Z-spectrum value at frequency ω that had the greatest CEST effect (M_s), the Z-spectrum value at frequency $-\omega$ (M_0), and each contrast agent concentration. The slope and intercept of this linear equation were used to calibrate the CEST effect with concentration ($1 - M_s/M_0$ vs [CA]).

$$\frac{M_s}{M_0} = \frac{1}{1 + \dfrac{n_{CA}[CA]T_1}{n_{H_2O}[H_2O]\tau_m}} \tag{1}$$

where M_s: water magnetization at steady state selective saturation of the contrast agent, M_0: water magnetization without saturation, n_{CA} and n_{H2O}: number of exchangeable protons on the contrast agent and water, respectively, [CA] and [H2O]: concentration of contrast agent and water, respectively, T_1: longitudinal relaxation time of the water in the presence of the contrast agent, and τ_m: average residence lifetime of the exchangeable proton on the contrast agent; $\tau_m = 1/k_{ex}$, where k_{ex} is the chemical exchange rate.

$$\frac{1}{T_1} = r_1[CA] + \frac{1}{T_{1w}} \tag{2}$$

where r_1: longitudinal relaxivity of the contrast agent and T_{1w}: longitudinal relaxation time of the water without the contrast agent.

$$\frac{\dfrac{M_0}{M_s} - 1}{[CA]} = \left(\frac{n_{CA}T_{1w}}{n_{H_2O}[H_2O]\tau_m}\right) - r_1T_{1w}\left(\frac{M_0}{M_s} - 1\right) \tag{3}$$

T_1 Relaxivity Measurements. Solutions were prepared with 0−50 mM Eu-DOTA-Gly, 0−50 mM Yb-DOTA-Gly, 0−0.3125 mM Eu-G5, and 0−1.875 mM Yb-G2. A spin−echo MRI pulse sequence was used to generate MR images of the solutions with TR times that ranged from 0.2 to 15 s. All other imaging parameters were identical to the parameters of the MRI studies of the CEST effect, and the temperature was maintained at 37 °C during the MRI study. The TR-dependent change in MR signal for each sample was analyzed with a single monoexponential function without a

(14) Woessner, D. E.; Zhang, S.; Merritt, M. E.; Sherry, A. D. Numerical solution of the Bloch equations provides insights into the optimum design of PARACEST agents for MRI. *Magn. Reson. Med.* **2005**, *53*, 790–799.

(15) Ali, M.; Liu, G.; Shah, T.; Flask, C. A.; Pagel, M. D. The Design of Multiple CEST MRI Contrast Agents for Molecular Imaging. *Acc. Chem. Res.*, in press.

constant term to determine the T_1 relaxation time. eq 2 was used to determine the r_1 relaxivity of the agent.

In Vivo CEST MRI. An in vivo study was conducted according to approved procedures of the Institutional Animal Care and Use Committee of Case Western Reserve University. A warmed solution of 1×10^6 MCF-7 mammary carcinoma cells (that were modified to express caspase-3 during apoptosis for purposes unrelated to this study) were injected subcutaneously into the rear flank of a 6-week-old female athymic NCR nu/nu mouse. The flank tumor was allowed to grow for 14 days until it reached a size of approximately 5 mm in diameter. The mouse was anesthetized with 2.0% isoflurane in oxygen carrier gas and secured to a customized cradle. A 26 G dental catheter was inserted into a tail vein to facilitate the injection of contrast agents while the mouse was in the MRI magnet. A phantom consisting of tapwater was taped to the mouse torso as a reference, and the lower flank of the mouse was tightly constrained to the cradle to prevent motion artifacts. Respiration and rectal temperature were continuously monitored and body temperature was maintained at 37.0 °C using warmed air and a computer-controlled temperature feedback system (SA Instruments, Inc.). After the MRI scan session, the mouse was removed from the MRI magnet and cradle and was allowed to recover from anesthesia.

MRI scans were performed with the same MRI scanner and MRI acquisition protocol used for solution studies. A series of MR images were acquired with saturation applied at +55 ppm (to detect Eu-G5) or −16 ppm (to detect Yb-G2). After acquiring three MR images at each saturation frequency, a solution of 0.04 mmol/kg Eu-G5 and 0.06 mmol/kg Yb-G2 was injected through the tail vein catheter in 50 μL volume, prepended by 60 μL of heparinized saline and followed by 90 μL of saline to flush the catheter. The total volume of 200 μL was manually injected in approximately 1 min. A series of MR images was then acquired for 30 min.

The CEST effect generated by each PARACEST agent was calculated by comparing the average water signal of the tumor at each postinjection time point (M_s) with the average of the water signal of the tumor for the average of the images before injection (M_0). The contrast-to-noise ratio, or the CEST-to-noise ratio in this type of experiment, must exceed $2\sqrt{2}$ in order to ensure that the contrast has a 95% probability of being real.[16] Although this statistical threshold for the CEST-to-noise ratio is based on Gaussian noise, this thresold is also valid for Rician noise present in this study due to the high signal-to-noise ratio of 133:1 for the MR image of the tumor before injection. To determine the noise level, the standard deviation of the MR signal of an image region that represented air was multiplied by $\sqrt{2}$ to account for the subtraction of two images before and after injection. Only pixels that reached this CEST-to-noise threshold for both Eu-G5 and Yb-G2 were used for subsequent analyses.

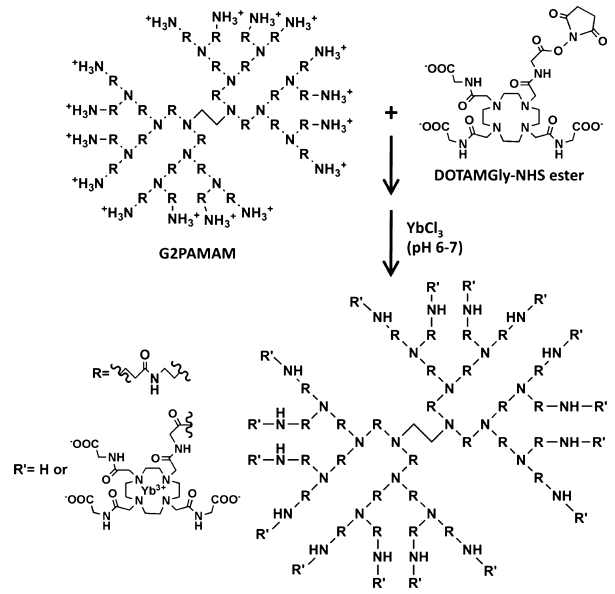

Figure 1. Schematic of the synthesis of the Yb-G2 PARACEST MRI contrast agent. A similar method was used to synthesize the Eu-G5 PARACEST agent.

The relative concentrations of the two CEST agents within the tumor tissue were determined by evaluating the ratio of eq 3 for each agent (eq 4). This concentration ratio of two CEST agents is a simple function of their CEST effects, exchange lifetimes, and number of exchangeable protons, assuming that the r_1 relaxivities of two CEST agents is negligible. The ratios of the exchange lifetimes of pairs of PARACEST agents were determined from the CEST effects of chemical solutions using eq 5.

$$\frac{[CA]_1}{[CA]_2} = \frac{\dfrac{\tau_{m1}}{n_{CA1}}\left(\dfrac{M_0}{M_s} - 1\right)_1}{\dfrac{\tau_{m2}}{n_{CA2}}\left(\dfrac{M_0}{M_s} - 1\right)_2} \text{ if } \frac{n_{CA}}{\left(\dfrac{M_0}{M_s} - 1\right)n_{H_2O}[H_2O]\tau_m} \gg r_1 \text{ for each agent} \quad (4)$$

$$\frac{\tau_{m1}}{\tau_{m2}} = \frac{n_{CA1}[CA]_1\left(\dfrac{M_0}{M_s} - 1\right)_2}{n_{CA2}[CA]_2\left(\dfrac{M_0}{M_S} - 1\right)_1} \quad (5)$$

Results

Synthesis and Characterization. DOTA-Gly was synthesized with excellent yield using a previously reported method. This product was conjugated to the surface of the PAMAM dendrimers through a EDC/NHS coupling method that was repeated twice to improve the conjugation yield (Figure 1). MALDI mass spectrometry analysis of the DOTA-Gly-conjugated G5PAMAM dendrimer indicated that

(16) Liu, G.; Ali, M.; Yoo, B.; Griswold, M. A.; Tkach, J. A.; Pagel, M. D. PARACEST MRI With Improved Temporal Resolution. *Magn. Reson. Med.* **2009**, *61*, 399–408.

Table 1. Sensitivities and Relaxivities of PARACEST MRI Contrast Agents

PARACEST agent	concentration to generate a 3.0% PARACEST effect: per lanthanide ion basis	concentration to generate a 3.0% PARACEST effect: per molecule basis	r_1 relaxivity (mM^{-1} s^{-1})
Eu-DOTA-Gly	1.62 mM	1.62 mM	0.0018
Eu-G5	1.85 mM	0.045 mM	0.107
Yb-DOTA-Gly	1.43 mM	1.43 mM	0.0115
Yb-G2	1.38 mM	0.242 mM	0.091

a range of 34−51 ligands were covalently attached to the surface of G5-PAMAM dendrimer, with a weighted average of approximately 41 ligands per dendrimer. A range of 5−7 ligands were present on the surface of G2-PAMAM dendrimer, with a weighted average of approximately 6 ligands per dendrimer. To ensure complete chelation of all DOTA-Gly ligands on the dendrimers, an excess of 1.2 equiv of $EuCl_3$ or $YbCl_3$ was used during the chelation procedure. Although an excess of lanthanide-chloride salts can be difficult to remove from the preparation and can be problematic for in vivo studies, the ability to dialyze the dentritic PARACEST agents to remove excess lanthanide-chloride salts greatly facilitated the preparation of these contrast agents for in vivo CEST MRI. ICP-mass spectrometry analysis was then employed to confirm the Eu(III) and Yb(III) content of the final products, and to calibrate the concentrations of solutions used for T_1 relaxivity and CEST sensitivity tests.

T_1 Relaxivity. The r_1 relaxivities of the PARACEST agents were measured with R^2 correlation coefficients greater than 0.99 for each analysis of eq 2 (Table 1). These r_1 relaxivities must meet the condition shown in eq 4 in order to use this equation to measure the ratio of concentrations of two PARACEST agents. These r_1 relaxivities meet this condition (i.e., are less than 15% relative to the left side of the condition listed in eq 4) for exchange lifetimes as long as 2 ms and CEST effects that are less than 33.5%, 15.1%, 42.9%, and 19.0% and for Eu-G5, Yb-G2, Eu-DOTA-Gly, and Yb-DOTA-Gly, respectively. Because the CEST effects that were measured in solution and in vivo were below these thresholds, the effects of r_1 relaxivities were neglected for analyses and interpretations of these CEST effects.

CEST Sensitivity. The CEST effects of each PARACEST agent were clearly evident in MR images of phantoms (Figure 2). The CEST effect was calibrated with concentration using Hanes-like CEST plots for each PARACEST agent (Figure 3A−D). The good linearity of each plot attested to the precision of this analysis method. The slope and intercept of these linear plots were used to construct a CEST-concentration calibration for each agent (Figure 3E−H). Based on these calibrations, Table 1 lists the concentrations on a per-molecule basis and on a per-lanthanide ion basis that are required to generate a 3.0% CEST effect for each agent (the description of the in vivo study listed below includes the rationale for comparing the PARACEST agents at this CEST value).

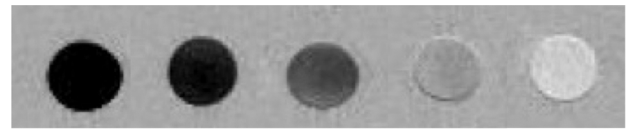

Figure 2. A parametric map of the CEST contrast of Eu-G5 at different concentrations was created by subtracting a MR image that was acquired with selective saturation applied at −55 ppm (i.e., M_0 in eq 1) from a similar image that was acquired with selective saturation applied at +55 ppm (i.e., M_S in eq 1).

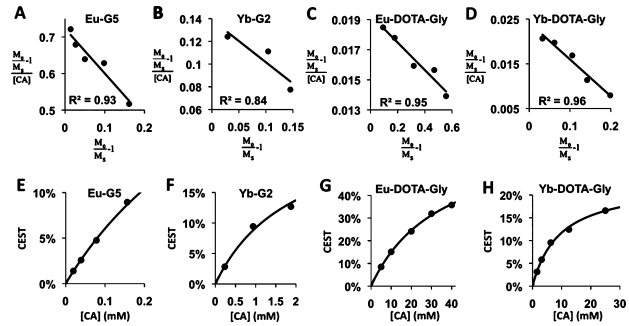

Figure 3. (A−D) The Hanes-like CEST plots of each PARACEST agent can be used to construct (E−H) calibrations of the CEST effects with concentrations for each agent.

Relative Chemical Exchange Lifetimes. The ratio of the exchange lifetimes of the dendritic PARACEST agents was determined using eq 5 for each pair of concentrations for the dendritic PARACEST agents. The average and standard deviation of this average of the exchange lifetime of Eu-G5 relative to Yb-G2 was 0.57 ± 0.03. Using the same analysis procedure, the exchange lifetime of Eu-G5 was measured to be 1.07 ± 0.03 times longer than that of Eu-DOTA-Gly, and the exchange lifetime of Yb-G2 was measured to be 0.92 ± 0.10 times as long as that of Yb-DOTA-Gly.

In Vivo CEST MRI. The MR images prior to the injection of contrast agents showed no significant changes, based on a $2\sqrt{2}$ CEST-to-noise threshold to ensure that a change in contrast has a 95% probability of being significant (Figure 4). Based on the 133:1 signal-to-noise ratio of the MR image of the tumor prior to injection, this CEST-to-noise threshold was reached at a CEST effect of 3.0%. The MR images after the injection of the contrast agents met this threshold at 2.46 min for Yb-G2 and 9.40 min for Eu-G5. This contrast steadily increased for each agent throughout the dynamic study, although the rate of increase noticeably slowed for Yb-G2 by the end of the study. The initial contrast change for both PARACEST agents occurred at the interior rim of the tumor and migrated toward the other side of the tumor during the dynamic imaging study. The ratio of the concentrations of Eu-G5 and Yb-G2 was determined at each time point starting at 9.40 min using eq 4, the measured CEST effects, the number of exchangeable protons of each agent, and the ratio of the exchange lifetimes determined from

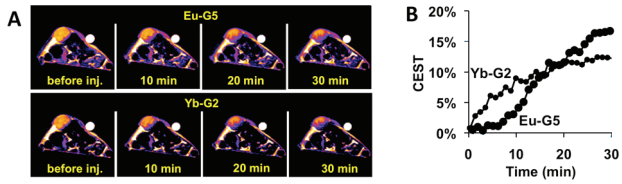

Figure 4. (A) Eu-G5 and Yb-G2 were injected iv into a xenograft flank mouse model of MCF-7 mammary carcinoma. Axial MR images were acquired by prepending a 20 μT saturation period for 2.25 s before a RARE-16 MR signal acquisition period. Selective saturation was applied at the PARACEST frequency of each agent. (B) The decrease in MR signal of the tumor after injection relative to the average MR signal before injection was used to measure the temporal changes of each CEST effect.

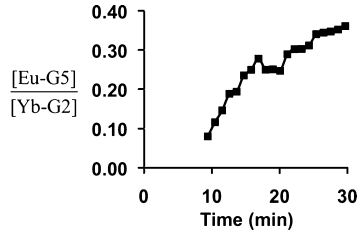

Figure 5. The temporal changes in the ratio of the concentrations of Eu-G5 and Yb-G2 dendritic PARACEST agents within the tumor tissue were determined from Figure 4B and eq 4.

the solution study (Figure 5). After the MRI scan session, the mouse quickly recovered from the anesthetic and showed no effects from the high-power selective saturation.

Discussion

CEST Sensitivity. The CEST sensitivity per lanthanide ion was essentially the same for the dendritic agents and monomeric agents, which agreed with previous reports with polymeric PARACEST agents (Table 1).[12,17] This similarity in sensitivity is attributed to the similarities of exchange lifetimes for the dendritic agents and monomeric agents. The payload of PARACEST agents on each dendrimer created an agent with greater CEST sensitivity on a per molecule basis. Based on the noise of the in vivo MR images, a CEST effect of 3.0% was required to ensure that a change in contrast has a 95% probability of being attributed to the accumulation of the contrast agent. The solution studies showed that concentrations of 0.045 and 0.242 mM Eu-G5 and Yb-G2, respectively, are required to generate a 3.0% CEST effect. These concentrations are achievable in vivo, based on previous studies with T_1 relaxation MRI contrast agents conjugated to PAMAM dendrimers and at standard injection concentrations of 0.04−0.06 mmol/kg of mouse body weight.[18] These concentrations should be considered as a minimum threshold for in vivo studies, because in vivo studies may require a greater concentration of a PARACEST agent relative to solution studies to generate the same CEST effect, as discussed below. For comparison, concentrations of 1.62 and 1.43 mM Eu-DOTA-Gly and Yb-DOTA-Gly are required to achieve a 3.0% CEST effect in solution, which may not be achievable in vivo with standard injection concentrations of 0.2 mmol/kg for small molecule MRI contrast agents. Therefore, the use of nanoparticles was critical for delivering sufficient payloads of agents for sensitive detection during the in vivo tumor study.

In Vivo CEST MRI. The change in image contrast of the tumor was assigned to the accumulation of the PARACEST agents in the tumor. This assignment was supported by the lack of significant contrast changes before injection of the agents and the generation of significant contrast changes after injection. The spatiotemporal matching of the constrast changes in the tumor caused by both saturation frequencies lended confidence that the changes in contrast were attributed to the PARACEST agents. However, the change in image contrast cannot be absolutely assigned to the CEST effect of the PARACEST agents. Chemical exchange may broaden the MR frequency distribution of the water, which may increase direct saturation of water.[19] No significant signal broadening in the NMR spectrum of the water peak was observed during our analyses of the effect of PARACEST agent concentrations, which indicates that the chemical exchange effect of the PARACEST agents on the direct saturation of water was negligible during the dynamic MR study. The PARACEST agents may also cause changes in magnetic field susceptibilities, which may shift the average MR frequency of the water that lead to changes in the direct saturation of water.[20] These magnetic field susceptibilities are estimated to be no higher than 0.5 ppm for 0.6 mM Eu-G5 and 2.5 mM Yb-G2. Considering that the direct saturation of in vivo water has a broad, super-Lorentzian line shape that is slowly varying between ±125 ppm, a 0.5 ppm shift caused by magnetic field susceptibilities is expected to have only a minor effect on selective saturations applied at 55 ppm and −16 ppm.[21] Yet, additional studies are warranted to validate that the change in image contrast can

(17) Wu, Y.; Zhou, Y.; Ouari, O.; Woods, M.; Zhao, P.; Soesbe, T. C.; Kiefer, G. E.; Sherry, A. D. Polymeric PARACEST Agents for Enhancing MRI Contrast Sensitivity. *J. Am. Chem. Soc.* **2008**, *130*, 13854–13855.

(18) Daldrup, H.; Shames, D. M.; Wendland, M.; Okuhata, Y.; Link, T. M.; Rosenau, W.; Lu, Y.; Brasch, R. C. Correlation of Dynamic Contrast Enhanced MR Imaging with Histologic Tumor Grade: Comparison of Macromolecular and Small-Molecular Contrast Media. *Pediatr. Radiol.* **1998**, *28*, 67–78.

(19) Haacke, E. M.; Brown, R. W.; Thompson, M. R.; Venkatesan, R. *Magnetic resonance imaging: physical principles and sequence design*; Wiley-Liss: New York, 1999; p 349.

(20) Peters, J. A.; Huskens, J.; Raber, D. J. Lanthanide induced shifts and relaxation rate enhancements. *Prog. Nucl. Magn. Reson. Spectrosc.* **1996**, *28*, 283–350.

(21) Henkelman, R. M.; Stanisz, G. J.; Graham, S. J. Magnetization transfer in MRI: a review. *NMR Biomed.* **2001**, *14*, 57–64.

be assigned to the CEST effect of the PARACEST agents during in vivo studies.[22−24]

Assessments of Relative Concentrations and Pharmacokinetics. Unfortunately, the solution-state calibration of CEST effects and concentrations (Figure 4) cannot be applied to convert the in vivo CEST effects to concentrations of each agent in the tumor. The T_1 relaxation time of the tumor tissue is less than the T_1 relaxation time of the solution, and the T_1 relaxation times of each location within the tumor were not determined in this study. More importantly, the concentration of in vivo water that may generate a CEST effect from the PARACEST agent, $[H_2O]_{CEST}$, is less than the ~55 M water concentration in solution, and $[H_2O]_{CEST}$ is unknown. The total in vivo water concentration is about 42 M, and only a subset of this water may interact with the PARACEST agent due to biological compartmentalization within the PARACEST time frame.[25] Some of this water may interact with exchangable protons of proteins, which further reduces $[H_2O]_{CEST}$.[26] Therefore, the solution-state calibration will underestimate the in vivo concentration of a PARACEST agent, and determinations of the absolute concentration of a PARACEST agent within in vivo tissues may be impractical.

Fortunately, these unknown $[H_2O]_{CEST}$ and T_1 relaxation times are equivalent for two PARACEST agents, so that the ratio of the concentrations of two PARACEST agents is independent of these unknown quantities. Thus, the concentration ratio can be determined from the ratios of their CEST effects (eq 4 and Figure 5). This ratio shows that the lower tissue permeability of the larger dendrimer causes less Eu-G5 to accumulate in the tumor tissue relative to Yb-G2, and the lower elimination rate of the larger dendrimer causes more Eu-G5 to be retained in the tumor over time. This ratiometric determination assumes that the ratio of the exchange lifetimes of the two PARACEST agents is the same in vivo and in solution. The effects of temperature and biological molecules on exchange lifetimes are expected to be similar for the two PARACEST agents, so that the magnitude of these effects on the ratio of exchange lifetimes may be reduced or eliminated.[27] The exchange lifetime of Yb-DOTA-Gly is pH-dependent, while the same lifetime of Eu-DOTA-Gly is independent of pH, so that pH may have some effect on the determination of the concentration ratio.[10]

In summary, this report has demonstrated that PARACEST MRI contrast agents can be used to measure the ratio of concentrations of two nanoparticles within an in vivo mouse model of mammary carcinoma. This concentration ratio was used to assess the relative pharmacokinetics of the two nanoparticles within the tumor tissue, which demonstrated the relatively lower tissue permeability and lower elimination rate of the larger nanoparticle, as expected. To further develop this methodology, further consideration should be given to the effects of magnetic field suceptibilities during in vivo MRI studies and the effect of pH on the ratiometric analysis. With these refinements, this methodology may provide accurate in vivo competitive assays that can identify the best nanoparticles for each biomedical application.

Abbreviations Used

CEST, Chemical exchange saturation transfer; DMSO, dimethyl sulfoxide; DOTA, 1,4,7,10-tetraazacyclododecane-*N*,*N*′,*N*″,*N*‴-tetraacetic acid; DOTA-Gly, 1,4,7,10-tetraazacyclododecane-*N*,*N*′,*N*″,*N*‴-acetamidoacetic acid; EDC, 1-ethyl-3-(3-dimethylaminopropyl) carbodiimide hydrochloride; EDTA, ethylenediaminetetraacetic acid; Eu(III), europium ion; $EuCl_3$, europium trichloride; Eu-DOTA-Gly, europium-(1,4,7,10-tetraazacyclododecane-*N*,*N*′,*N*″,*N*‴-acetamidoacetic acid); Eu-G5, $(Eu\text{-}DOTA\text{-}Gly)_{41}$-G5PAMAM contrast agent; G2PAMAM, second generation PAMAM dendrimer; G5PAMAM, fifth generation PAMAM dendrimer; H_2O, water; ICP, inductively coupled plasma; MALDI, matrix assisted laser desorption/ionization; MES, 2-(*N*-morpholino)ethanesulfonic acid; MRI, magnetic resonance imaging; MWCO, molecular weight cutoff; NaOH, sodium hydroxide; NHS, *N*-hydroxysuccinimide ester; PAMAM, polyamidoamine; PARACEST, paramagnetic chemical exchange saturation transfer; RARE, rapid acquisition with relaxation enhancement; SEC-HPLC, size exclusion chromatography-high performance liquid chromatography; TR, repetition time; Yb(III), ytterbium ion; $YbCl_3$, ytterbium trichloride; Yb-DOTA-Gly, ytterbium-(1,4,7,10-tetraazacyclododecane-*N*,*N*′,*N*″,*N*‴-acetamidoacetic acid); Yb-G2, $(Yb\text{-}DOTA\text{-}Gly)_6$-G2PAMAM contrast agent.

Acknowledgment. The authors would like to thank the Case Center for Imaging Research and the Department of Macromolecular Science and Engineering at Case Western

(22) Sun, P. Z.; Farrar, C. T.; Sorensen, A. G. Correction for artifacts induced by B0 and B1 field inhomogeneities in pH-sensitive chemical exchange saturation transfer (CEST) imaging. *Magn. Reson. Med.* **2007**, *58* (6), 1207–1215.

(23) Shah, T.; Ali, M. M.; Liu, G.; Pagel, M. D.; Flask, C. A. FISPCEST: A Rapid, Acquisition for Dynamic Detection of CEST/PARACEST Activity. *Proc. Int. Soc. Magn. Reson. Med.* **2008**, 3067.

(24) Stancanello, J.; Terreno, E.; Delli Castelli, D.; Cabella, C.; Uggeri, F.; Aime, S. Development and validation of a smoothing-splines-based correction method for improving the analysis of CEST-MR images. *Contrast Media Mol. Imag.* **2008**, *3* (4), 136–149.

(25) Zhou, R.; Pickup, S.; Yankeelov, T. E.; Springer, C. S., Jr.; Glickson, J. D. Simultaneous measurement of arterial input function and tumor pharmacokinetics in mice by dynamic contrast enhanced imaging: effects of transcytollemal water exchange. *Magn. Reson. Med.* **2004**, *52* (2), 248–257.

(26) Li, A. X.; Hudson, R. H. E.; Barrett, J. W.; Jones, C. K.; Pasternak, S. H.; Bartha, R. Four-pool modeling of proton exchange processes in biological systems in the presence of MRI-paramagnetic chemical exchange saturation transfer (PARACEST) agents. *Magn. Reson. Med.* **2008**, *60*, 1197–1206.

(27) Englander, S. W.; Downer, N. W.; Teitelbaum, H. Hydrogen Exchange. *Annu. Rev. Biochem.* **1972**, *41*, 903–924.

Reserve University for access to a MRI scanner and NMR spectrometer, respectively. The authors would also like to thank Prof. Nancy Oleinick at Case Western Reserve University for access to the genetically modified MCF-7 mammary carcinoma cells. This research was supported by the Northeastern Ohio Small Animal Imaging Resource Center, an NIH funded program (R24CA110943).

Supporting Information Available: Details of the synthesis of DOTA-Gly and characterization of dendritic PARACEST agents, and Figure S1 showing MALDI mass spectra of $(DOTAM\text{-}Gly)_{41}$-G5PAMAM and $(DOTAM\text{-}Gly)_6$- G2PAMAM. This material is available free of charge via the Internet at http://pubs.acs.org.

MP900040U